#

ACQUISITION OF THE NESTED 3D SEISMIC SURVEY AT HARVEY

Final report

ANLEC R&D Project 7-1213-0224

Prepared by:

M. Urosevic, S. Ziramov, R. Pevzner

CURTIN UNIVERSITY

13/10/15

#

CONTENTS#

ACKNOWLEDGEMENTS

The authors acknowledge financial assistance provided through Australian National Low Emissions Coal Research and Development (ANLEC R&D). ANLEC R&D is supported by Australian Coal Association Low Emissions Technology Limited and the Australian Government through the Clean Energy Initiative. The authors would also like to acknowledge contributions to the South-West Hub Flagship project by the Western Australian Department of Mines and Petroleum (including the Geological Survey of Western Australia). We are grateful to Linda Stalker (CSIRO) and Dominique van Gent (DMP) for their help and guidance that made this project possible.

EXECUTIVE SUMMARY

A large 3D seismic survey at the South West CO2 Hub Project near Harvey, covering an area of approximately 130 km^2, was acquired in the first quarter of 2014. The survey proved to be of great importance for characterisation of the reservoir, mapping the main structures and key geological interfaces. However, small to medium shallow structures were less clearly imaged in this survey as the recording geometry was adjusted for the regional investigations and greater depths, which is between 2 km and 3 km. To investigate if the imaging of the shallow structures could be improved, a high-resolution 3D survey was undertaken. The survey was centred at the Harvey-4 well. The main objective was to establish the complexity of the shallow structures in 3D that are of a high importance to the dynamic modelling. In the next stage of research, recorded logs and VSP data are to be used to calibrate the new high resolution seismic.

In December 2014, a Nested 3D survey was conducted with light vehicles, two UNIVIB trucks and a seismic crew of eight people. A single source - single receiver recording combination was used. Signal to noise ratio and resolution were improved by utilisation of long, broadband sweeps and high fold. Close to 1600 seismic source positions were acquired over 5 days. The whole survey including mobilisation and demobilisation lasted 11 days. Seismic receivers utilised single and 3-component geophones arranged into an odd-even receiver line pattern. The extra-wide tires mounted onto the UNIVIB sources were used in order to leave no impact on the ground.

Data from the nested survey were processed at Curtin University using both standard and relative-amplitude-preserving workflows. Full 3D pre-stack time migration processing produced images of high resolution and quality. New seismic images allow for the interpretation of faults, previously unidentified in the regional 3D survey. Some of the smaller throw faults can be interpreted to propagate to the near surface. Complex faults are interpreted to surround Harvey-4 well. It is likely that the Harvey-4 borehole trajectory has an intersection with one of the fault planes. It should be also observed that even deep, large-scale faults are better imaged with the new high-resolution survey than the regional survey. Based on the results achieved we propose that similar surveys should precede drilling in order to characterise complex structures and optimise borehole drill location and well design. The fault complexity revealed by the new data suggests that much higher data density and resolution are required for accurate structural analysis and reservoir characterisation that can be determined from the regional 3D survey.

Greater fault complexity than identified in the regional seismic was expected based on the study of Langhi et al. (2012) who, based on the power law strain distribution, demonstrated that a large part of the overall strain was unaccounted for. The new high res 3D may be able to help explain where this strain is likely to be located relative to the larger observable faults.

Table of abbreviations

Abbreviation	Description
3D	Three-dimensional survey
UV	UNIVIB (INOVA, 24, 000 Lb) – NGL owned and operated
RP	Receiver point
VP	VIbration point, also known as shot point (SP)
CMP	Common mid-point (often wrongly expressed as common depth point)
CSP	Common source point
AGC	Automatic gain control
NMO	Normal move-out
m	Meter
km	Kilometre
s	Second
ms	Millisecond
kg	Kilogram
S/N	Signal to noise ratio
DMO	Dip move-out or partial pre-stack migration
PSTM	Pre-stack time migration
PRA processing	Preserved relative amplitude processing

Data acquisition, processing and analysis of the Nested 3D Harvey seismic survey

In this report we describe the work accomplished, methodology applied and the results achieved with the high-resolution experimental 3D seismic survey centred around the Harvey-4 well location in Perth near Bunbury. The survey was termed “Nested” as it was shot within the existing regional commercial 3D seismic survey area. The project utilised NGL UNIVIB seismic vibration sources and for the first time a Sercel state-of-the-art hybrid acquisition system – UNITE® (www.Sercel.com/products). Over 2300 geophones were deployed for the survey, the highest ever channel count deployed by the Department of Exploration Geophysics, Curtin University. Results of the survey are presented in this report.

Seismic expression of the underground shallow geology is analysed and also compared to the previous 3D large survey which utilised conventional large size vibrator trucks. The main findings are discussed in light of the project objectives and future research directions are proposed.

Introduction

The main objective of the high-resolution 3D survey at the Harvey-4 well was to obtain a better image of the shallow fault zones and to inform the risk assessment for the CO_2 storage complex. In order to achieve this we acquired a very high density, high resolution 3D survey that we called “Nested” as it is situated within the area covered by the large regional site characterisation commercial 3D seismic. The nested survey is specifically targeting the top ~1km part of the subsurface and is placed around the location of the Harvey -4 well. This well is of high value to the geo-sequestration project as is of a critical data acquisition importance for computation of the dynamic model for the larger area.

The large scale 3D seismic survey was acquired in the summer of 2014 and it provided very good information of the subsurface structures and main stratigraphic units. However due its large size the regional 3D survey was not dense enough to obtain high-resolution imaging of the shallow geological features. This part will be provided by the additional high-resolution nested 3D survey. The structural information that will be derived from this new survey will provide data that will enable an updated interpretation of a recent fault history analyses to be undertaken. It was hoped that the nested high-Data Acquisition chapter – included resolution 3D survey would produce a crisp image of the structures surrounding the Harvey-4 well and define fault tips and the termination points.

The opportunity to use the latest state-of-the-art seismic data acquisition and processing technologies was expected to produce:

1. A clearer image of the shallow subsurface targeting additional detail of fault structures, informing project risk assessment.
2. Validation of the high-resolution data acquisition and processing techniques and protocols and informing the location of planned shallow wells. This is hoped to be achieved through identification of

additional, smaller scale faults associated to the larger faults observed in the commercial regional 3D survey. Possible presence of a more complex fault system was also suggested by Langhi et al. (2012).

3. Detailed characterisation of the near surface around Harvey-4 well.

4. Validation of the “infill approach” where conventional and high-resolution seismic methods are combined to produce high quality images for all depths. This approach is rarely utilised in the seismic exploration practice. In the case of SW Hub investigations at Harvey, the “high resolution infill approach” is of a particular interest due to difficulties associated with obtaining the permission for seismic survey execution. Moreover the high data density utilised in the high-resolution survey permits so-called “vertical” infill that is provides geological information of the shallow structures that are not recorded with a sparse 3D regional seismic survey geometry.

5. Investigation into the potential use of converted shear waves for an improved fault characterisation workflow.

State-of-the-art seismic equipment consisting of Sercel 428 and a wireless UNITE® system (www.Sercel.com/history) available to the NGL researchers was used for the seismic acquisition campaign. This included two NGL acquired INOVA Univibe seismic sources (Urosevic et al., 2014). This equipment is capable of producing wide band, high-density seismic data which will enable production of high resolution images of the underground formations.

Data Acquisition

Initial acquisition design incorporated a hybrid recording system utilising a single 3D patch approach with over 3000 active seismic cannels. However permission in regard to land access for a portion of the planned 3D area was not granted in time of the data acquisition. Consequently only 2330 channels, along 21 receiver lines, were needed to cover the new, reduced acquisition area. Two UNIVIB tracks were used in flip-flop shooting pattern. This involves two vibrators moving along two different source lines. Such approach enables much higher production as no time is lost in waiting the vibrator truck to position itself at the desired location. Other equipment included trailer-mounted fuel supplies unit (800 L), two trucks, three crew 4WD vehicles and one passenger car used to commute from Perth to the site. The mobilisation started on the 1st of December 2014. Receiver spread deployment started late on 2nd of December following the surveyors and meetings with KD1 (land access and stakeholder management) group, affected landowners and DMP representatives. The survey crew started one ahead to be able to position the flags along the first eight receiver lines. As the cable and the wireless equipment started the survey crew continued with additional lines ahead of the seismic equipment deployment. Seismic crew consisted of 8 people, all from the Department of Exploration Geophysics. Three PhD students and 5 staff members were fully occupied with the survey.

21 receiver lines were laid in a way that every second line utilised three-component (3C) geophones. Separation for both 1C and 3C geophones was 15m. The 3C geophones were linked to a UNITE® wireless

system, while the 1C geophones were linked to Sercel 428X system. All receiver lines were deployed, programmed and tested by the 5th of December. Survey statistic is shown in Figure 1.

Shooting, after sweep testing started the on 6th of December utilising a flip-flop strategy (2 viberoseis trucks). Sweep parameters included a single sweep with the frequency range of 6-150Hz and a sweep duration of 24 seconds. Some 1558 shots were fired in 4 ½ days. Demobilisation started by December 12th and finished by lunchtime. All the equipment were de-mobilised and stored in Curtin University shed in Perth by December 15th.

The actual survey geometry, as accomplished including all executed shots is shown in Figure 2. Land access permission was not obtained for the shaded purple area therefore additional four shots lines were deployed north of this zone to partially compensate for the loss of fold. The idea was to preserve the highest fold possible around the Harvey-4 well.

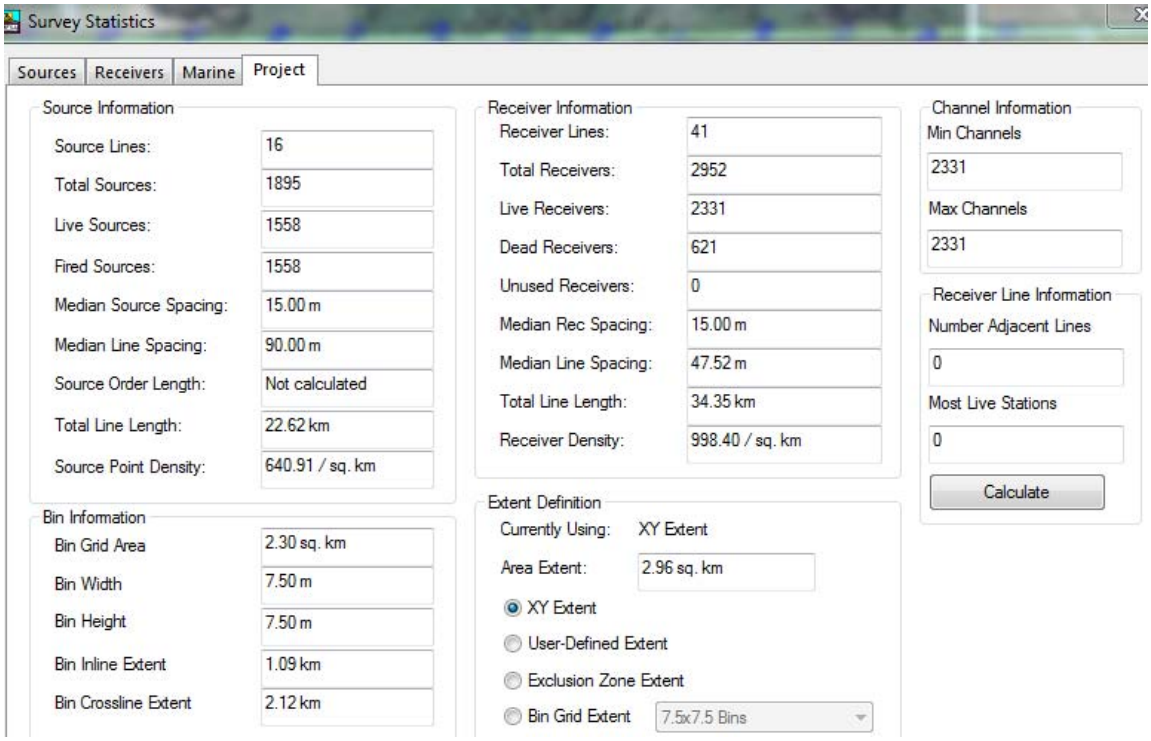

Figure 1. Survey statistics: 21 receiver lines were positioned in a way that every second line had 3-component geophones active. Hence the total number of live channels was over 2300.

Unfortunately permission was not granted across entire planned 3D area, which affected the data fold and imaging of shallow structures in the north-east part of the study area. The fold around the Harvey-4 well was unaffected by the ground restrictions. The data in that area contains near offsets necessary for proper imaging of shallow structures.

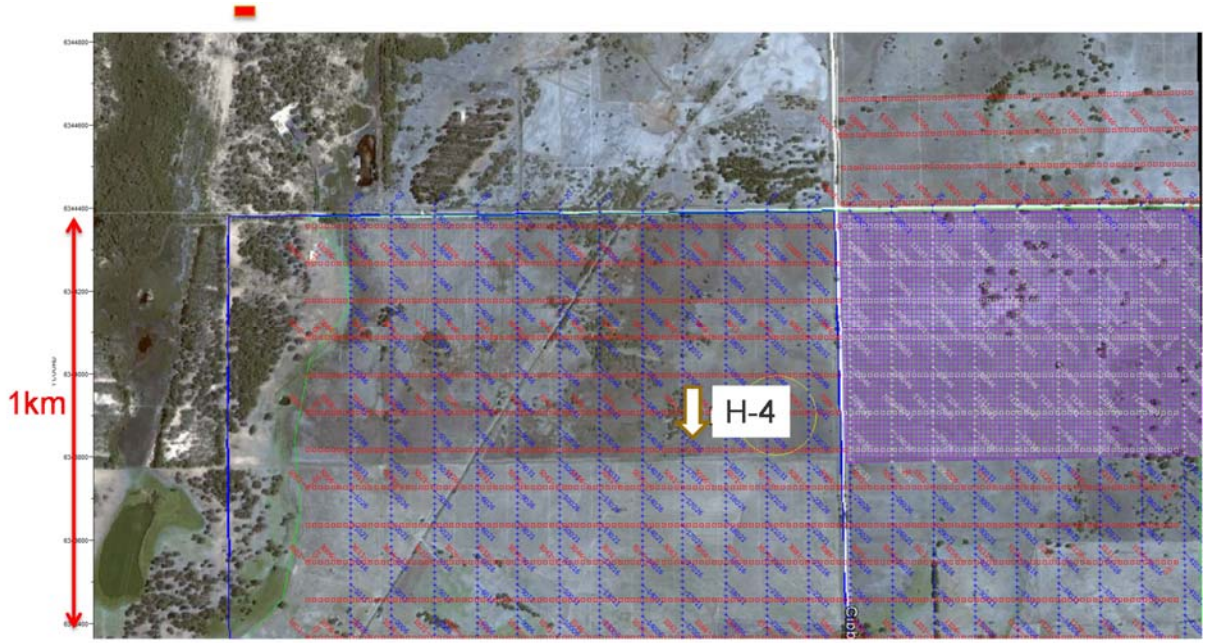

Figure 2. Final distribution of the sources (red) and receivers (blue). Shaded purple zone is the exclusion area. An additional four source lines (north of the purple shaded area) were added to compensate for this. Harvey-4 well is indicated with the white arrow.

Data processing

Data preparation for processing required harvesting of the UNITE data (3-component) and then concatenating it with the Sercel 428 data. The subsequent pre-processing workflow is displayed in Table 1. The main objectives of this pre-processing stage were the application of static corrections and the signal-to-noise ratio (SNR) improvement so that detailed velocity analysis could better accomplished. For that purpose this stage of processing utilised robust scaling. Final processing deployed surface consistent amplitude scaling and relative amplitude preservation. This approach is often referred to as PRA processing which stands for Preserved Relative Amplitude processing. More specifically the PRA processing incorporates the application of the following steps:

- Spherical divergence correction (simple velocity function)
- Shot root mean square energy equalisation (single scalar per shot)
- Surface consistent amplitude correction (Taner and Koehler, 1981)
- Offset balancing (single scalar)

Vertical component data were loaded into the SeisSpace processing system and reformatted to internal format. Note that three component data is available for every odd receiver line. In this study we concentrate on vertical (Z-component) data. 3D geometry (Figure 3) information was extracted from the SPS files that were created by the acquisition system. The final or post-acquisition SPS files contain exact survey layout related to the active geophone spread for each vibration point (VP). Following the 3D geometry assignment

to the database and the subsequently trace headers, detailed examination and verification of its accuracy was performed. The data were binned using the nominal bin size of 7.5mx7.5m, which resulted in a fold map shown in Figure 4. The fold around the Harvey-4 well is in excess of 150 fold. The high fold was essential for combating ambient noise (construction equipment around the well, farm activities, wind). The single sweep – single geophones combination used for acquisition were aimed at preservation of the broad band of the signal but it cannot suppress ambient noise. Here we used the high fold to achieve the noise suppression.

The next processing step was editing of the bad and/or noisy traces. For implementation of single receiver per station technique, the quality of geophone planting is essential. As this was clear to everyone in the seismic crew the planting “success rate” was very high. Only a handful of traces were eliminated from further processing due to poor coupling. Trace editing was conducted with an automatic routine. Compensation for the amplitude loss was first applied then the root mean square (RMS) threshold energy value was computed. Traces with abnormally high amplitude values (typically 10:1 amplitude ratio computed for the selected time window) were eliminated from further processing. Some traces contained noise bursts. For that purpose TDF noise rejection was used to isolate noise bursts and replace them with the median spectral amplitudes calculated from 21 adjacent traces. The frequency range was set to 0-125 Hz.

Procedure	Parameters
Data conversion	**SEG-D data Input and conversion to Seispace internal format**
Geometry assignment	**Applied from SPS files**
Binning	**Bin size 7.5m x 7.5m**
Correlation	**Sweep correlation**
Trace Editing	**Kill bad traces**
Air Blast Attenuation	**Attenuation mode for air velocity at 331 m/s**
Elevation Statics	**Final datum elevation – 40 m, Replacement Velocity – 2500 m/s**
Residual Static	**Application of residual statics**
Deconvolution	**Minimum phase predictive Operator length – 120ms, predictive distance 8ms Operator 'white noise' level – 0.1%**
Band-pass Filtering	**4-10-150-250 (Hz)**
Surface wave noise attenuation	**Velocity 1200m/s, frequencies 4-40Hz**
Automatic Gain Control (display purposes)	**500ms**

Table 1: Pre-processing Flow Chart.

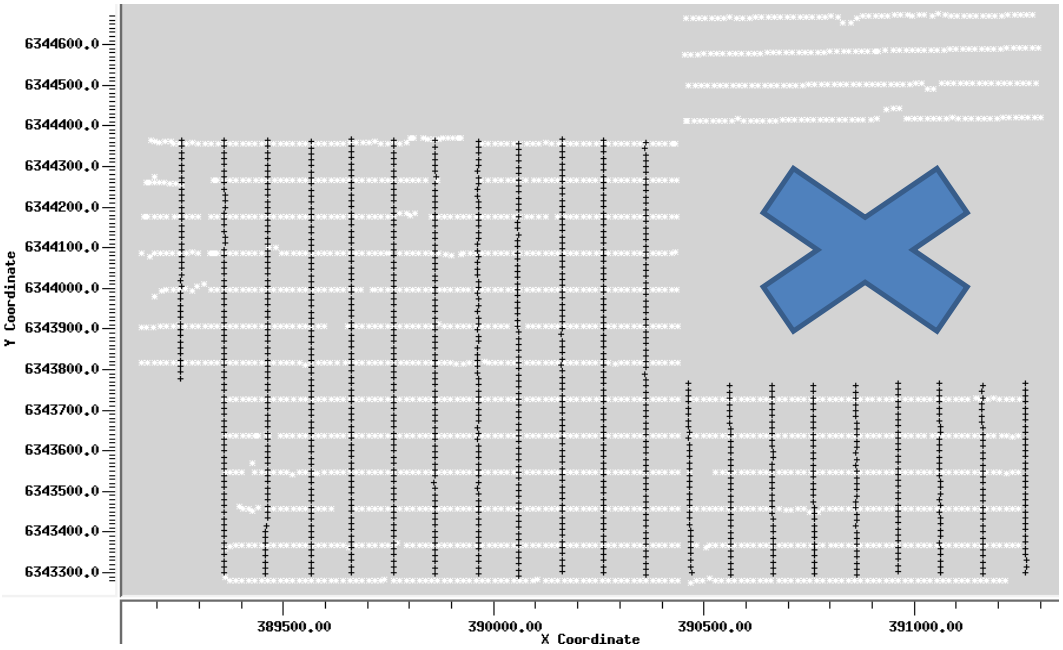

Figure 3. Survey layout: source lines are shown in white, receiver in black. No-go zone is denoted with blue-X. This is the same layout as in Figure 2 except the background image has been removed so that shot and receiver irregularities related to the obstacles on the ground can be observed. The obstacles cause delays in the survey execution.

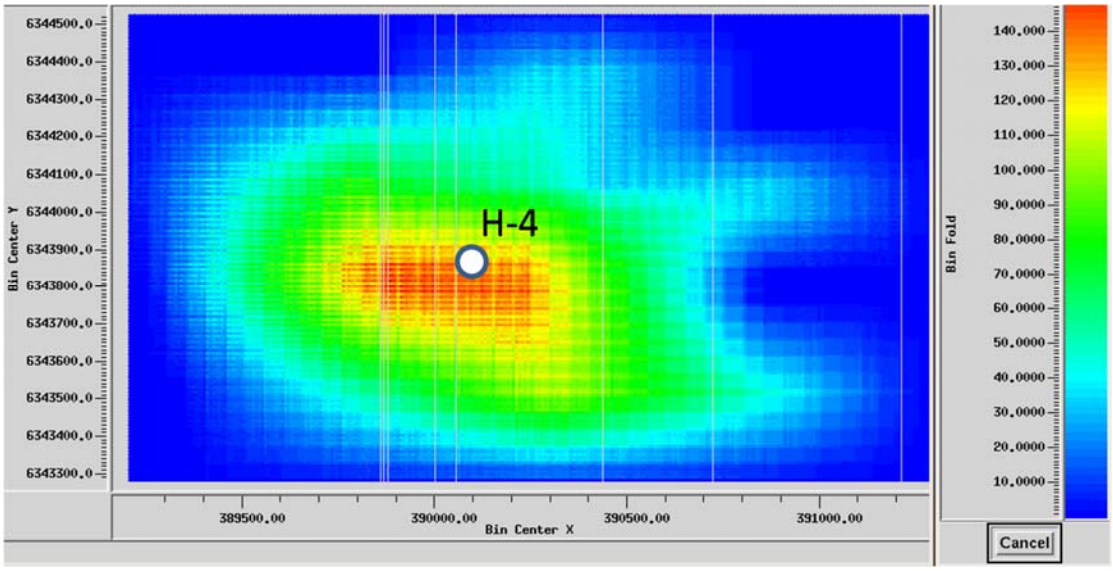

Figure 4. CMP fold coverage. The Harvey-4 well is situated close to the centre of the highest coverage. The fold distribution map is greatly affected by the no access zone as shown in Figure 2 (shaded area).

Gentle topographic variations over the survey area, from 10m-42m, resulted in a low magnitude static correction. In fact most of the area is nearly flat. For the selected seismic datum of 40 m, and a replacement velocity of 2500 m/s, total variations in delay times were below 5 ms (Figure 5). Following the application of elevation statics, surface consistent residual statics (SCRS) were applied. The total magnitude was below 5 ms. Hence the first break picking for the standard computation of refraction statics was not required. An alternative method that was applied to the Harvey 2D high-resolution data, termed surface consistent LMO refraction statics (Hatherly et al., 1994), was not attempted due to large gaps in the surface geometry.

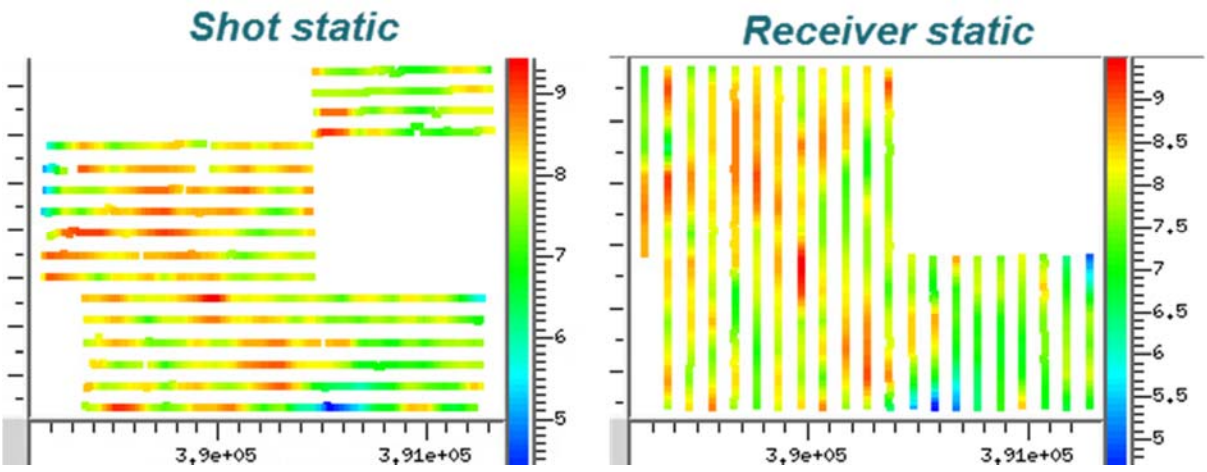

Figure 5. Elevation statics for all VPs (left) and all receiver positions (right).

Signal-to-noise ratio improvement

The ambient noise, as discussed before, is suppressed through the process of stacking; the effectiveness is proportional to the fold of data. The stacking is not so effective in suppressing the coherent noise that is source-generated noise. The main types of coherent noise are: air blast, surface or Rayleigh waves and refracted waves (P and converted S-waves). Additional problems come from the multiple reflections or simply “multiples”. An air blast attenuation routine (2D operator) using an air-wave velocity of 331 m/s was applied for attenuation of waves propagating across the receiver spreads through the air. Surface waves were attenuated with the frequency-wavenumber (F-K) based routine that operates on the apparent slopes. The frequency range was limited to the surface wave frequency range that minimised the signal damage. To precondition data for this 2D filtering operation, each 3D shot was decomposed into a sequence of 2D shots, arranged by the receiver line number and sorted from maximum negative to maximum positive offset. Subsequently we applied a deconvolution to attenuate short period multiples and improve the shape of the wavelet. This also increased temporal resolution. After testing different algorithms, a predictive deconvolution was selected. The deconvolution operator length was initially estimated using an autocorrelation function computed across selected shots. The performance was judged in two ways: a) by visual inspection of the continuity and reflectivity of the primaries and b) by the shape of the autocorrelation curve after application of different deconvolution routines and their parameters. Eventually an operator length of 120 ms and operator predictive distance of 8ms was chosen. Deconvolution was followed by a broad band-pass filter (6-16-160-200 Hz). The purpose of this filter was to remove low frequency deconvolution artefacts such that high frequencies were unaffected.

For the continuation of the processing leading into velocity analysis and imaging we went along two paths:

A) A non-preserved amplitudes approach through application of robust scaling (automatic gain control or AGC). The amplitude equalisation level is inversely proportional to the window size where the average RMS value is determined. We used a standard window of 500 ms, which made poorly reflective events more “visible” and improved velocity analysis. Selected raw and pre-processed shot records are displayed in Figures 6 and 7, respectively. In Figure 6, totally refracted P, converted S-waves, surface waves and air blast dominate the entire data space; reflections cannot be observed.

B) Preserved amplitude processing (PRA). Performance of this approach is judged by comparing the final image quality to the amplitude non-preserved image or so call AGC image. The criteria included both reflectivity and continuity in space and time.

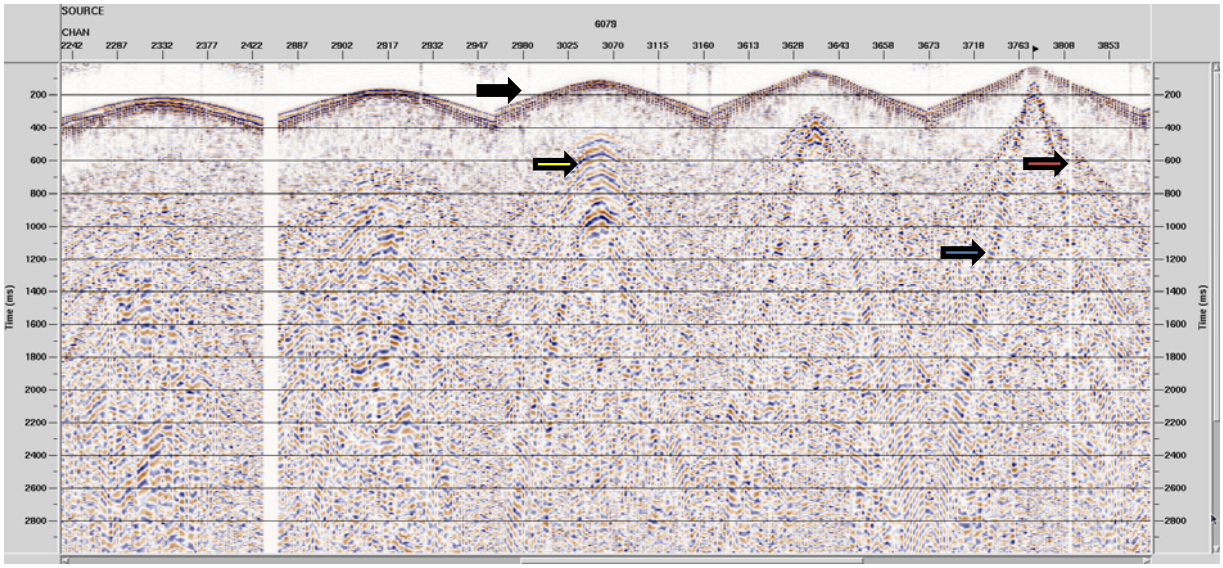

Figure 6. Raw shot gather: black arrow – refracted P-waves, Yellow arrow-surface waves, red arrow-refracted converted waves, blue arrow-air blast.

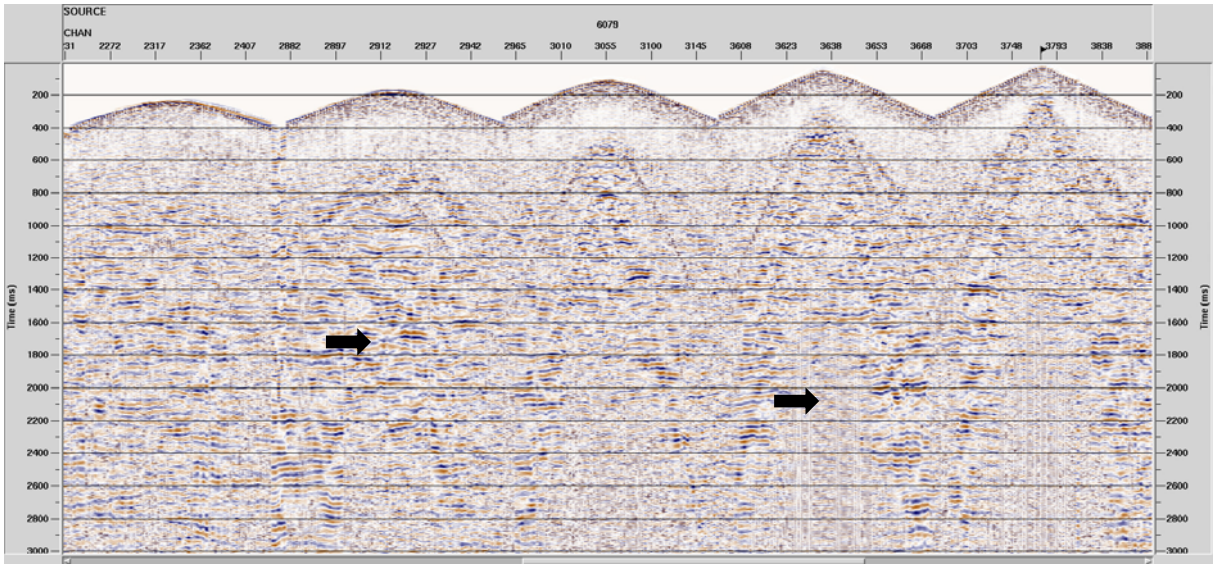

Figure 7. Pre-processed shot gather: primaries can be observed (some are mark with black arrows).

Velocity analysis

Velocity analysis, particularly semblance-based interactive velocity analysis, requires further SNR improvement. For that purpose, the band-pass filter was temporarily narrowed to 8-14-50-70 Hz. This reduced the contribution of random noise at the high end of the spectra. Further signal enhancement was achieved by building 3D super-gathers using 5x5 CDPs in the in-line and cross-line directions, respectively.

Two velocity analysis passes were made. The initial velocity field was built upon the information provided by the 2D reflection seismic survey, acquired in 2013. Regular offset distributions used for the 2D seismic

profile produced a reliable velocity field in the processing plane. So we used this field as a guide. The 2D velocity field was subsequently extended to 3D space and refined to better condition the data for residual static corrections. An example of the velocity spectra (semblance) or so-called interactive velocity (IVA) analysis is illustrated in Figure 8.

The second velocity field was constructed after the application of a dip move-out correction (DMO), that is, after dip-dependency of the stacking velocities was accounted for. This field was used for stacking and post-stack migration. It was also used as an initial velocity field for pre-stack time migration (PSTM). In the first iteration, the PSTM was conducted on a pre-processed dataset in the offset domain. The second that was also the final velocity iteration was computed on image gathers and then used for the final run of the post-stack time migration.

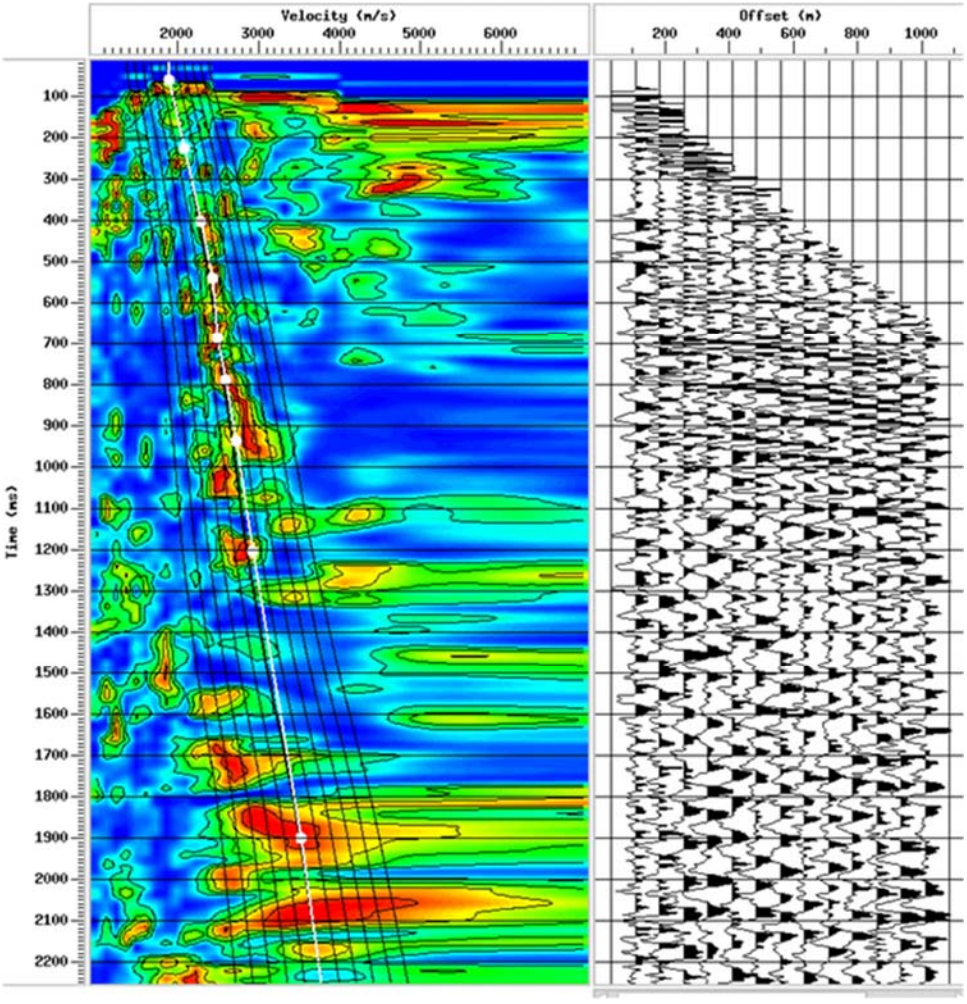

Figure 8. Interactive velocity analysis. On the left is the semblance panel with 11 velocity functions overlaid (black curves). The central function (white curve) is the guide function “borrowed” from the high-resolution 2D line. A super gather is shown on the right. Reflections are clearly visible to 1.1 seconds.

Post-stack migration

The post-stack migration flow is shown in Table 2. Characteristic for this flow are applications of DMO, robust scaling (AGC), F-XY deconvolution and filters to enhance the signal. These types of images are often utilised for the initial structural analysis rather than for lithological analysis and/or inversion, which would require Preserved-amplitude processing (PRA) images and preservation of the wide frequency band in the data.

Two 3D post-stack migration algorithms were tested: Kirchhoff and Phase-shift (PS) migration. This product had a dual purpose. It was to be used for the initial structural analyses and also the help estimate the quality of the subsequent post- stack migration images. For that purpose we evaluated the reflection strength and continuity in the post- stack migration images against post-stack migration images (stream a). Selected in-line and cross-line from PS cubes are shown in Figure 9. Numerous faults can be particularly well identified in the West-East direction (cross-line direction). It is also apparent that the near surface has not been particularly well imaged.

Finally note that the gaps in the near offsets (eastern side) are due to access restrictions (see also Figure 2).

Procedure	Parameters
Data input	**Pre-processed dataset**
NMO Iteration I	**Velocity field I (from 2D survey)**
DMO to Gathers 3D Iteration I	**Offset binning: 30/60/2060**
Velocity analysis	**Compute velocity field II**
NMO Iteration II	**Velocity field II**
DMO to Gathers 3D Iteration II	**Offset binning: 30/60/2060**
60% starch mute	**Post-NMO top mute**
Band-pass filter	**5-15-150-200 (HZ)**
3D stack	**Normalisation scalar 0.5**
FXY deconvolution	**Window 200/800ms**
Post-stack migration	**Velocity field II converted to interval velocities**
Display Filters	**5-25-90-150 (HZ)**
Depth conversion	**Velocity field II converted to average velocity**
SEGY output	**Standard SEG Rev1**

Table 2: Post-stack Migration Flow Chart.

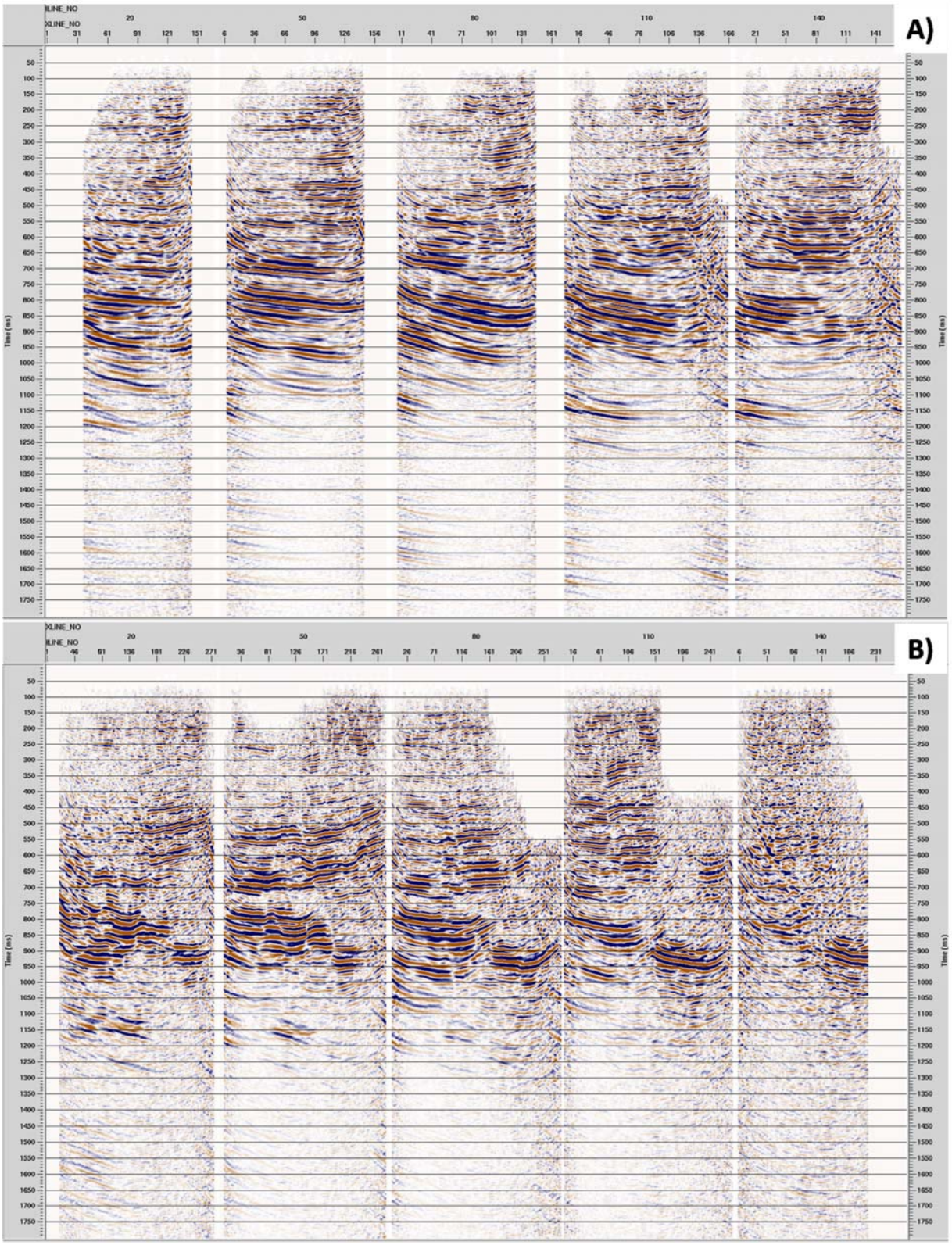

Figure 9. Post stack 3D migration: A) selected in-lines and B) Selected cross-lines. Faults are easier to identify in cross-line direction (West-East)

Pre-stack migration

Pre-stack time migration (PSTM) was utilised for several reasons: a) to improve imaging of complex structures for all depths but particularly near surface and b) to test the image quality in terms of continuity of geological interfaces that could be used at some stage for sequence stratigraphy interpretations. Two PSTM runs were accomplished. The first version utilised a robust (AGC) scaling while the second version used preserved-amplitude processing (PRA). The hope was that the PRA PSTM version would produce sufficient image quality that it can be utilised at some later stage for acoustic impedance inversion, when well logs from Harvey-4 became available for calibration. The principal difference between AGC and PRA cubes is that the latter has surface consistent amplitude scaling which amounts to the application of a single scalar per trace. The AGC assigns every sample in each trace a different scaling factor. Hence the AGC approach equalises the reflectivity in both space and time. The PRA is compensating the differences in source-receiver response (coupling and source energy level) using consistency and source-receiver reciprocity principles (Taner and Koehler, 1981). The effect of the energy decay with offset is also considered, while the effect of the underground geology is incorporated through the selection of a time window for computation of the surface consistent scalars. The first PSTM run utilised DMO velocities.

The first PSTM run with AGC scaling utilised the following stages:

- Step 1: Initial velocity preparation and a 1st pass of pre-stack time migration;
- Step 2: Residual velocity model modification;
- Step 3: Final migration;

Step 1 utilised the RMS velocity field inferred from the velocity analysis of the DMO corrected gathers. The actual imaging using the Kirchhoff integral solution (Gardner et al., 1974; French, 1975; Schneider, 1978) was done on pre-processed offset gathers, without the DMO correction. Typically, many of the reflection events in the image gathers, produced by the first pass of migration, are not properly imaged. This points to the errors in the initial velocity model that will require refinement of the velocity model in an iterative manner.

Step 2 analyses velocity errors by examining the “flatness” of the events in image gathers. These so-called residual velocity errors are corrected as “the move out correction”. This analysis makes changes to the original velocity model that will more precisely flatten the image gathers. In turn, flat image gathers guarantee the highest stack energy output, which translates to sharp and coherent migrated images.

Since our initial velocity model was already a reasonably good approximation of the true velocities, a single iteration in step 2 was sufficient to produce correct image gathers. Step 3 then simply included the execution of PSTM with a final velocity field. A post-migration process applied to image gathers included elimination of extrapolated migration swings (manual mute of image gathers) and band-pass filtering. The workflow for pre-stack migration is shown in Table 3. PRA PSTM included part of the workflow shown in black in Table 3.

Procedure	Parameters
Data input	**Pre-processed dataset**
Velocity datuming	**Moving seismic and velocities to final datum**
PSTM run I	**Offset binning: 30/60/2060, Velocity field II**
Velocity analysis	**Compute velocity field III**
PSTM Iteration I	**Offset binning: 30/60/2060, Velocity field III**
60% stretch mute	**Post-NMO top mute**
3D stack	**Normalisation scalar 0.5**
FXY deconvolution	**Window 200/800ms**
SEGY output	**Standard SEG Rev1**

Table 3. PSTM workflow.

PSTM results

Two PSTM runs, so-called AGC and PRA, are compared using a common band-pass Ormsby filter with a frequency specification of 5/25Hz – 90/150Hz, somewhat narrower than the original sweep bandwidth that was 6Hz-150 Hz. This filter was also used in the post-stack migration workflow (see Table 2 and Figure 7) to enhance the reflector continuity. In Figures 10 and 11 we compared the results obtained with AGC and PRA pre-stack migration runs. The expectation was that due to irregular geometry and in particular offset distribution, the AGC will produce an image of better application to structural analysis. It turned out that PRA processing produced superior results in overall imaging, particularly in the shallow depths (0ms-500ms). Even deeper, (700-1100 ms) the PRA processing produced superior fault image clarity. In Figures 12 and 13 we compare PRA PSTM results using a 5/25Hz-90/150Hz filter and a practically open filter (broad band filter). The differences are very subtle suggesting that the contribution of the very low and very high frequencies is not great. However, careful inspection shows that some details in the shallow part are better imaged with the open filter. Below 500 ms, the filtered version seems to have less migration artefacts and produces images that are perhaps easier for interpretation.

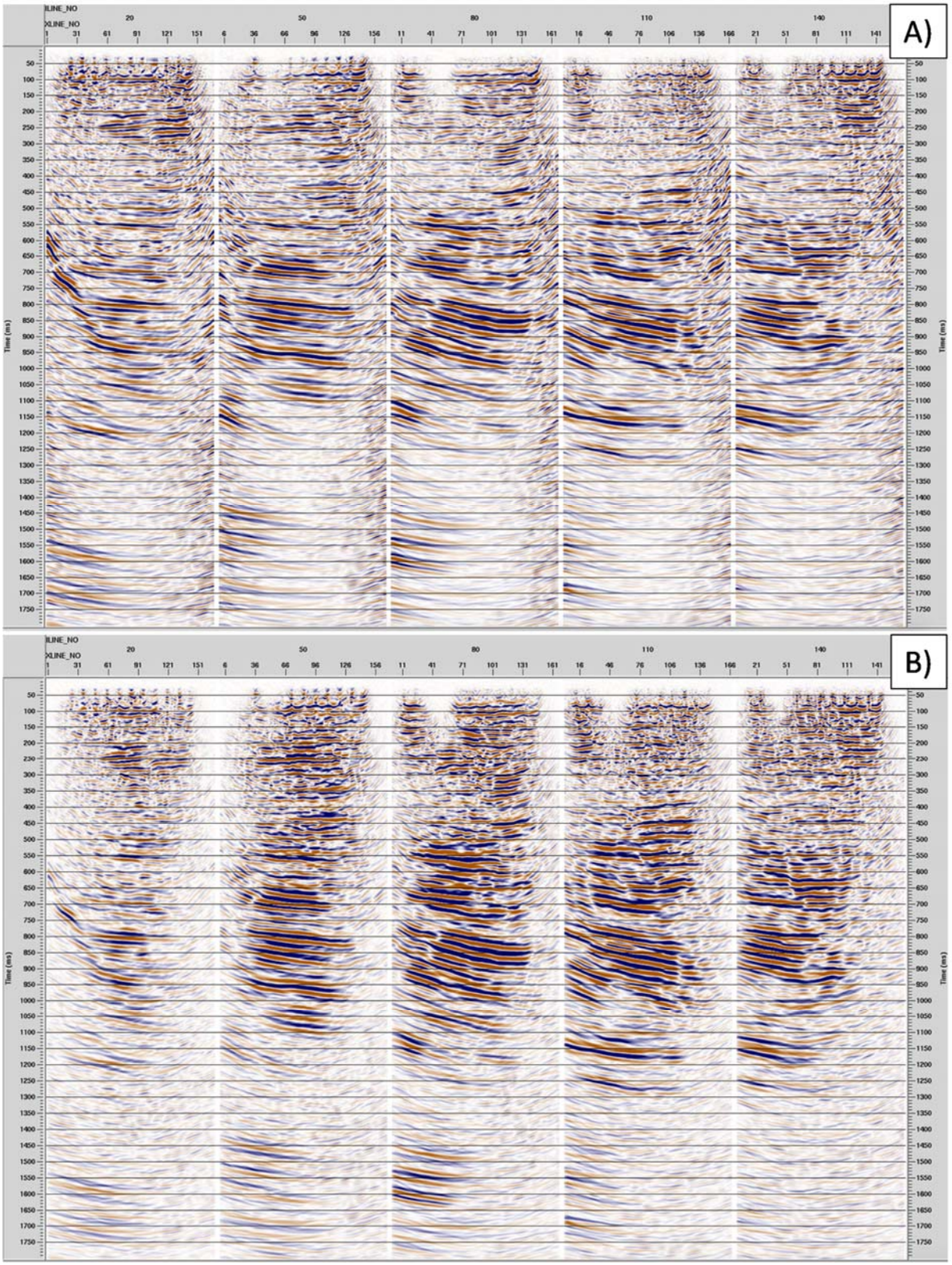

Figure 10. Selected PSTM in-lines from: A) AGC cube and B) PRA cube. Both cubes were filtered with a “narrow” band-pass filter: 5/25Hz-90/150Hz.

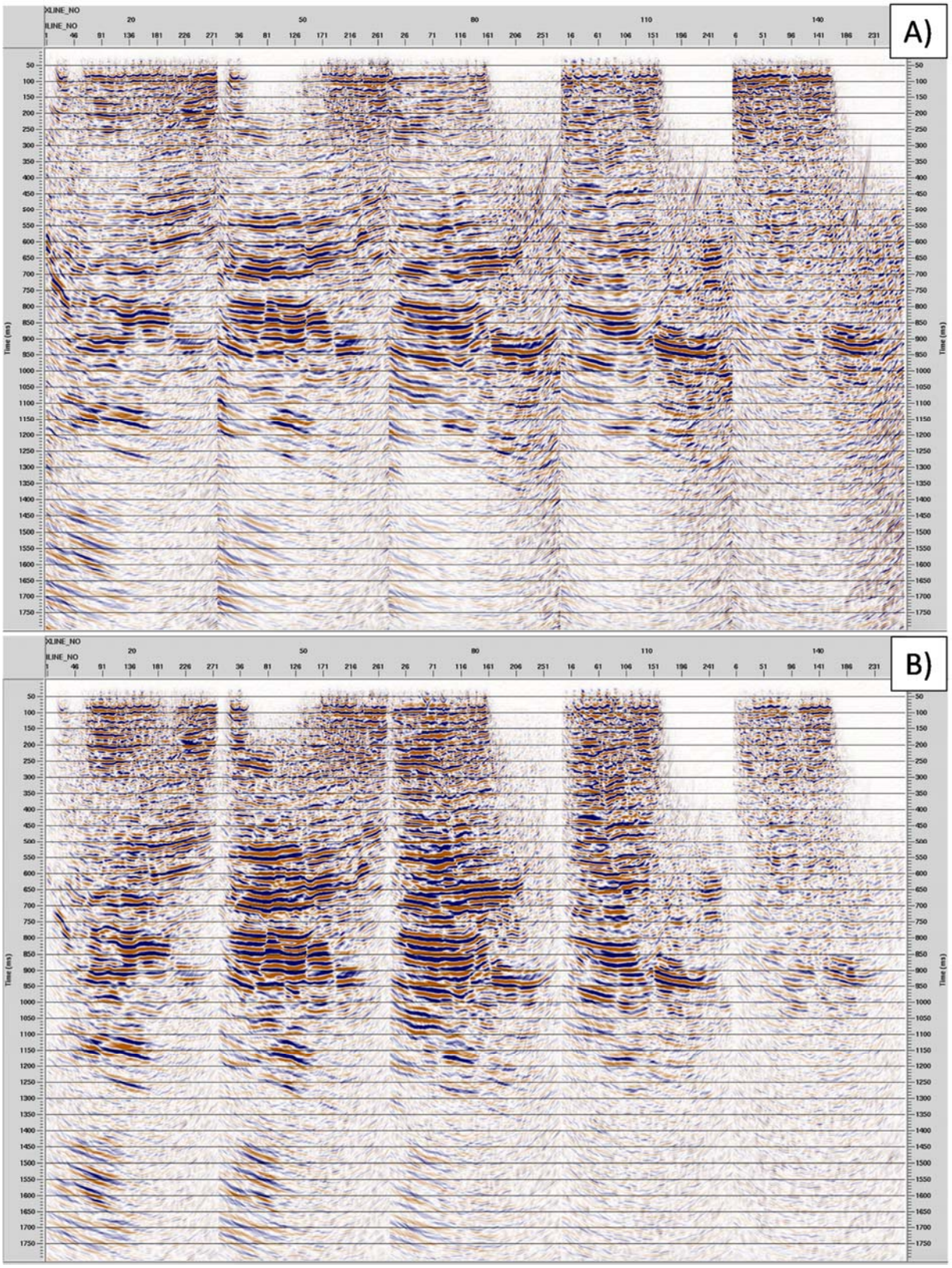

Figure 11. Selected PSTM cross-lines from: A) AGC cube and B) PRA cube. Both cubes were filtered with BP: 5/25Hz-90/150Hz.

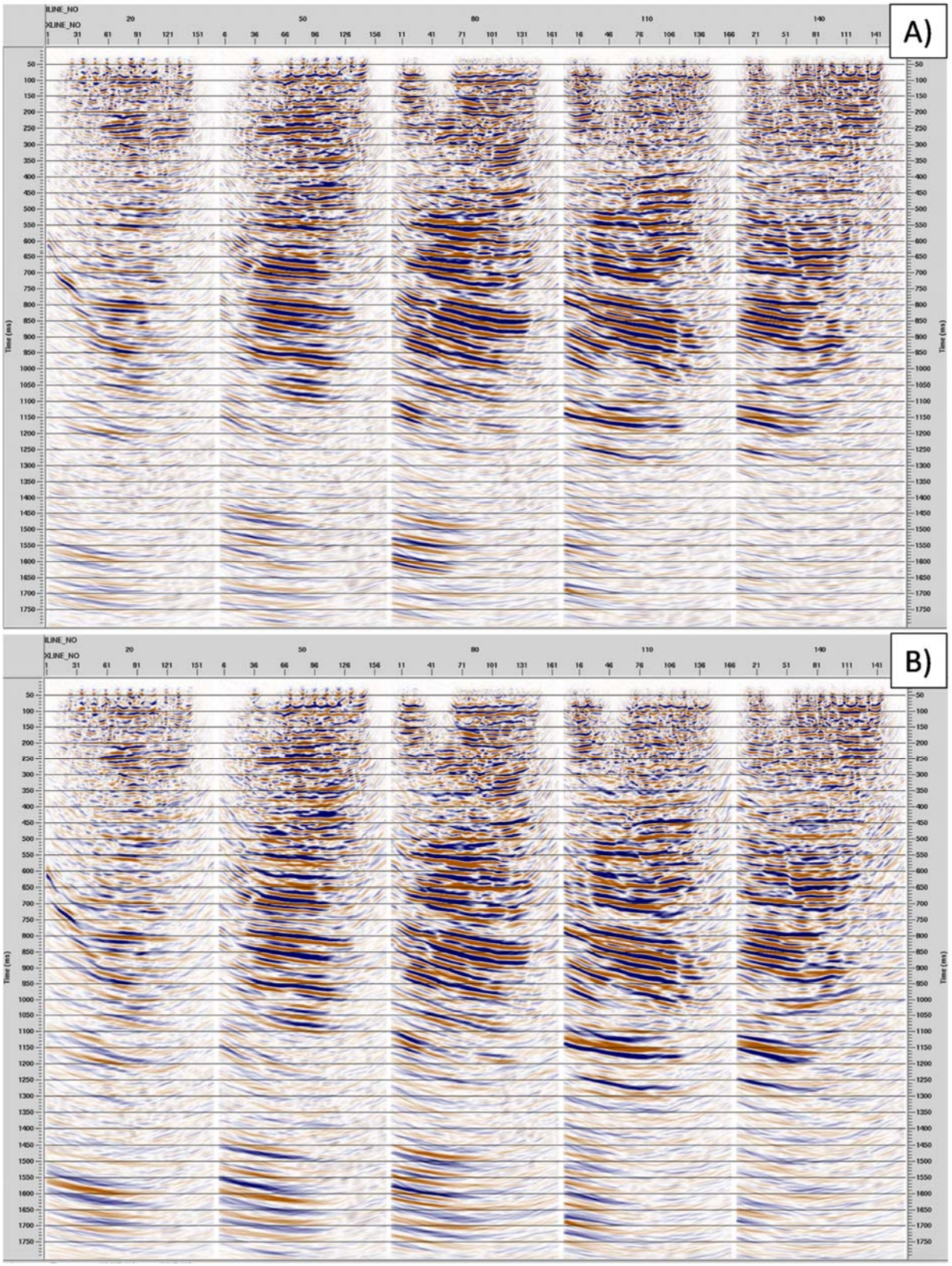

Figure 12. Selected PSTM PRA in-lines from: A) Filtered cube (5/25Hz-90/150Hz) and B) cube with broad- band filter (5/15Hz-150/200Hz).

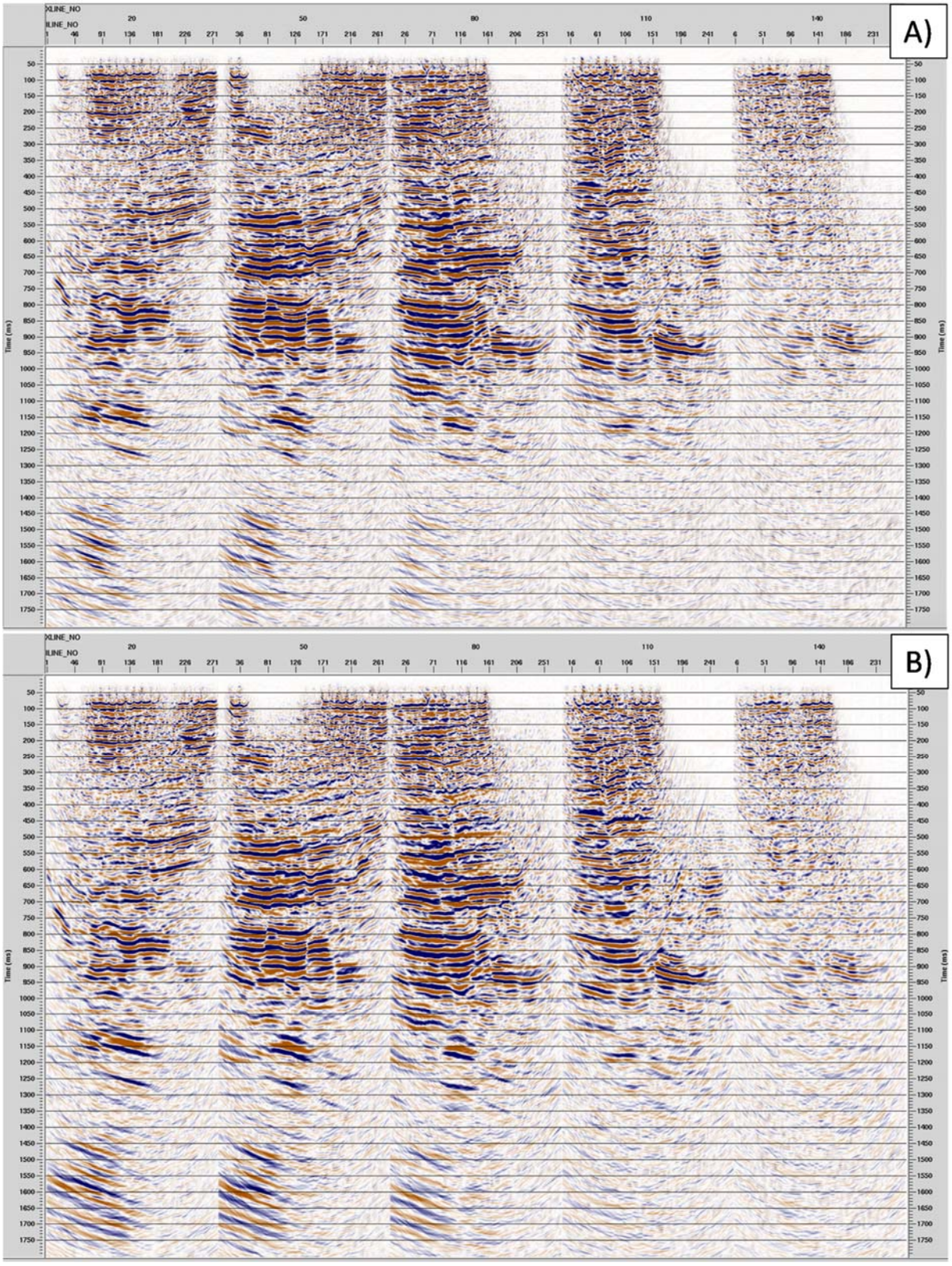

Figure 13. Selected PSTM PRA cross-lines from: A) Filtered cube (5/25Hz-90/150Hz) and B) cube with broad-band filter (5/15Hz-150/200Hz).

Initial comparison of large and Nested 3D surveys

The main objective of the Nested 3D survey was to produce high-resolution images of the shallow structures (0-1000 m). One way of verifying that the objective was achieved is through a direct comparison with the regional 3D Harvey survey. An initial comparison was made using a chair display. One such example is shown in Figure 14. A brief inspection of images shown clearly demonstrates that the objectives were achieved and that the Nested 3D survey contains new geological details, not observable in the previous regional survey. Further investigation and comparison utilised 2D image planes extracted from the 3D volume, which are easier to comprehend and observe in detail. One of the objectives was to compare fault expression in the two data sets. For that purpose we first enhanced the faults through the

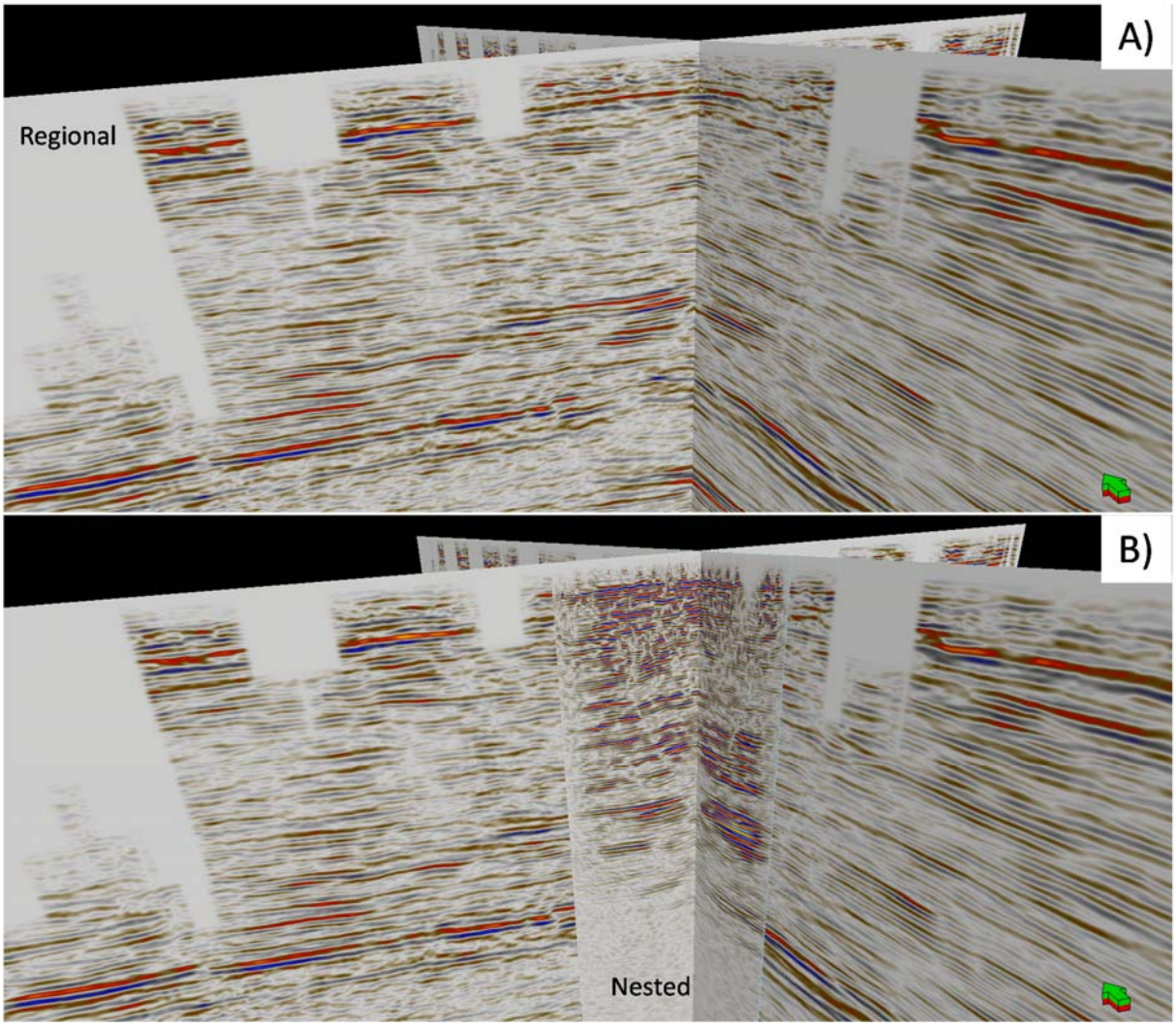

Figure 14. Harvey 3D: A) regional survey and B) regional survey with 3D nested survey inserted. Nested 3D survey demonstrated higher resolution and better overall expression of the shallow geology.

computation of a so-called minimum similarity cube. Firstly, time slices showing clear fault expression were selected. Then the in-line and cross-line passing through the fault trace were used for comparison. This is

demonstrated in Figures 15-18. From these pictures it is clear that the new high resolution 3D has provided new information about the shallow structures, not seen in the regional data, despite the ¼ gap in the survey. It is also clear that the dense survey grid has provided more fidelity of fault traces down to approximately 1.5 km depth, and possibly deeper.

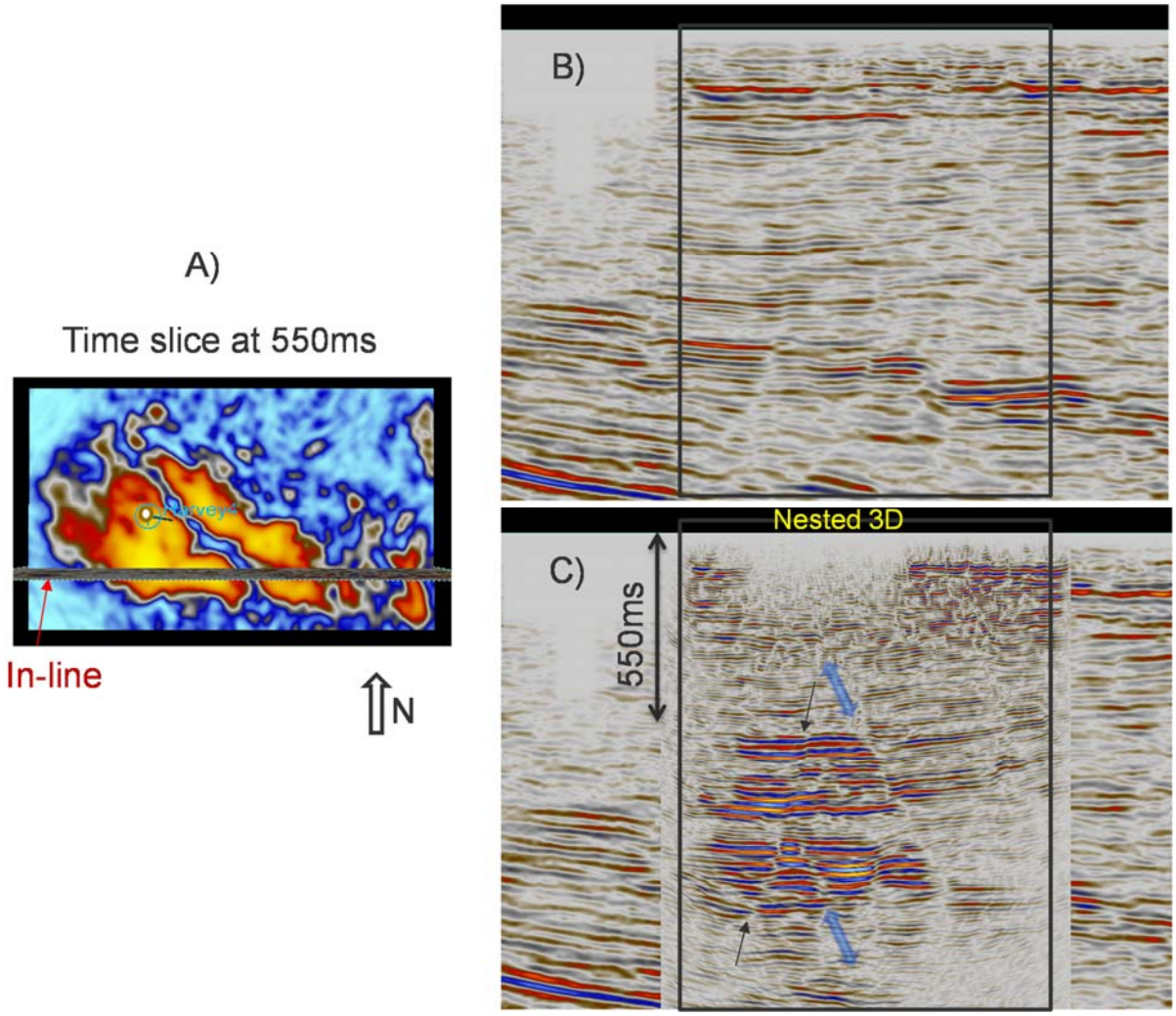

Figure 15. 3D survey comparison: A) Time slice through similarity section, B) Regional Harvey 3D and C) Nested 3D (PSTM cube) inserted into the rectangular area. The location of the inline section shown is marked in A). The Harvey 4 borehole is shown as a green circle. The white in-fill small circle is added to enhance the borehole position only in this display. The blue transparent double arrow is used to denote “new” fault images, not seen in the regional data. The black arrow denotes where fault is expressed with much better clarity in the Nested 3D.

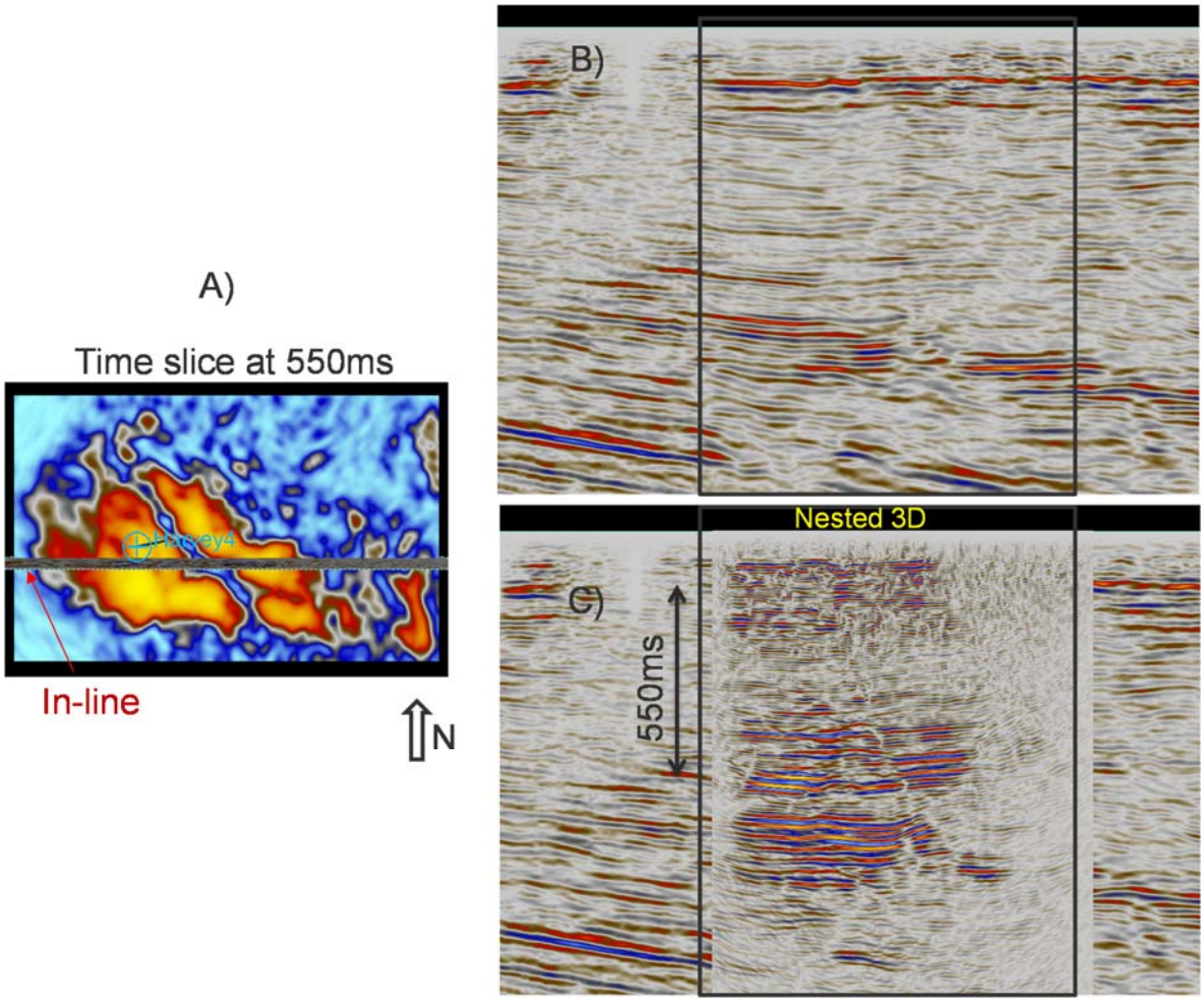

Figure 16. 3D survey comparison: A) Time slice through similarity section, B) Regional Harvey 3D and C) Nested 3D (PSTM cube) inserted into the rectangular area. The location of the inline section shown is marked in A). The blue transparent double arrow is used to denote “new” faults, not seen in the regional data. The black arrow denotes where fault is expressed with much better clarity in the Nested 3D.

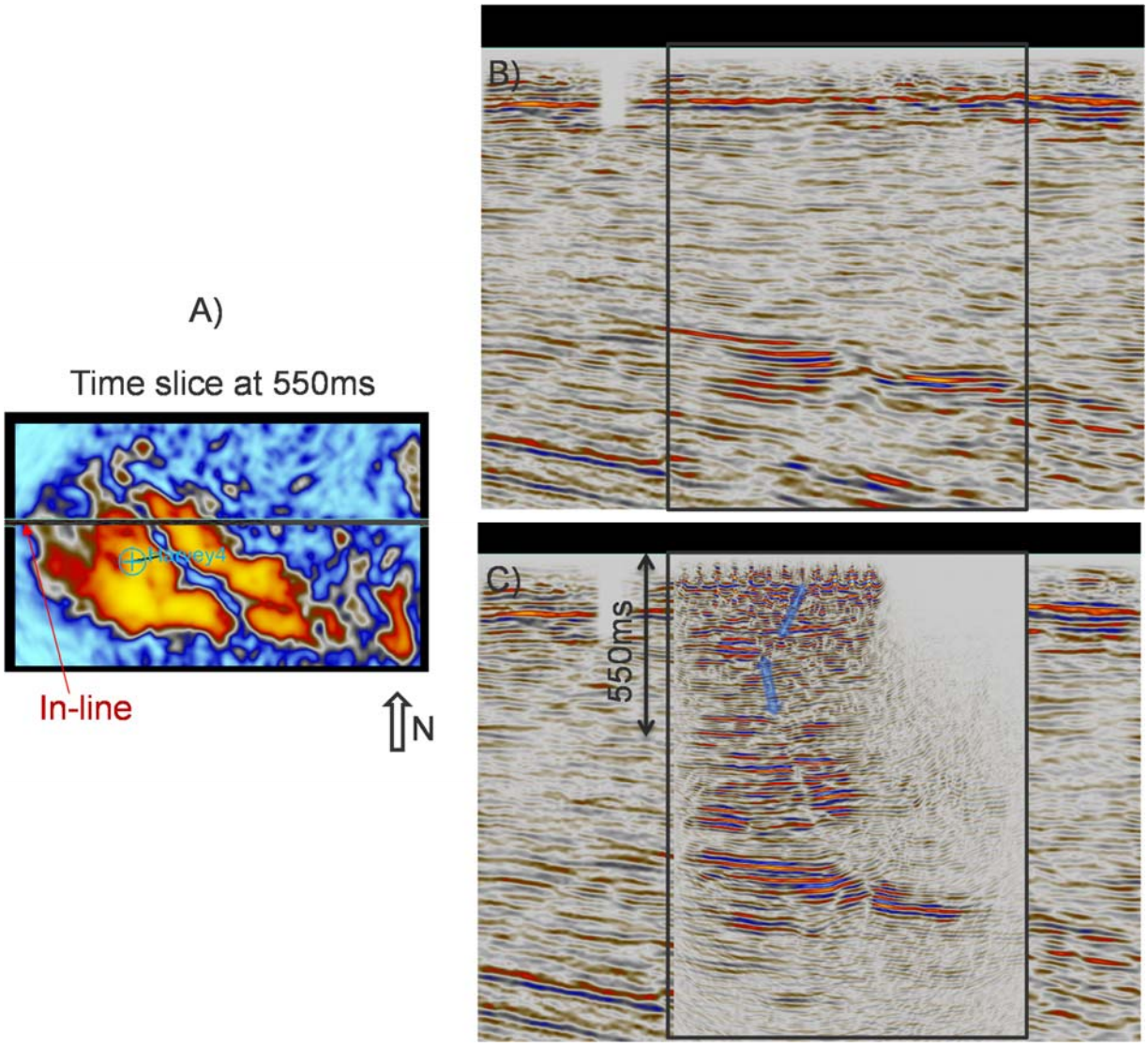

Figure 17. 3D survey comparison: A) Time slice through similarity section, B) Regional Harvey 3D and C) Nested 3D (PSTM cube) inserted into the rectangular area. The location of the inline section shown is marked in A). The blue transparent double arrow is used to denote “new” faults, not seen in the regional data. The black arrow denotes where fault is expressed with much better clarity in the Nested 3D.

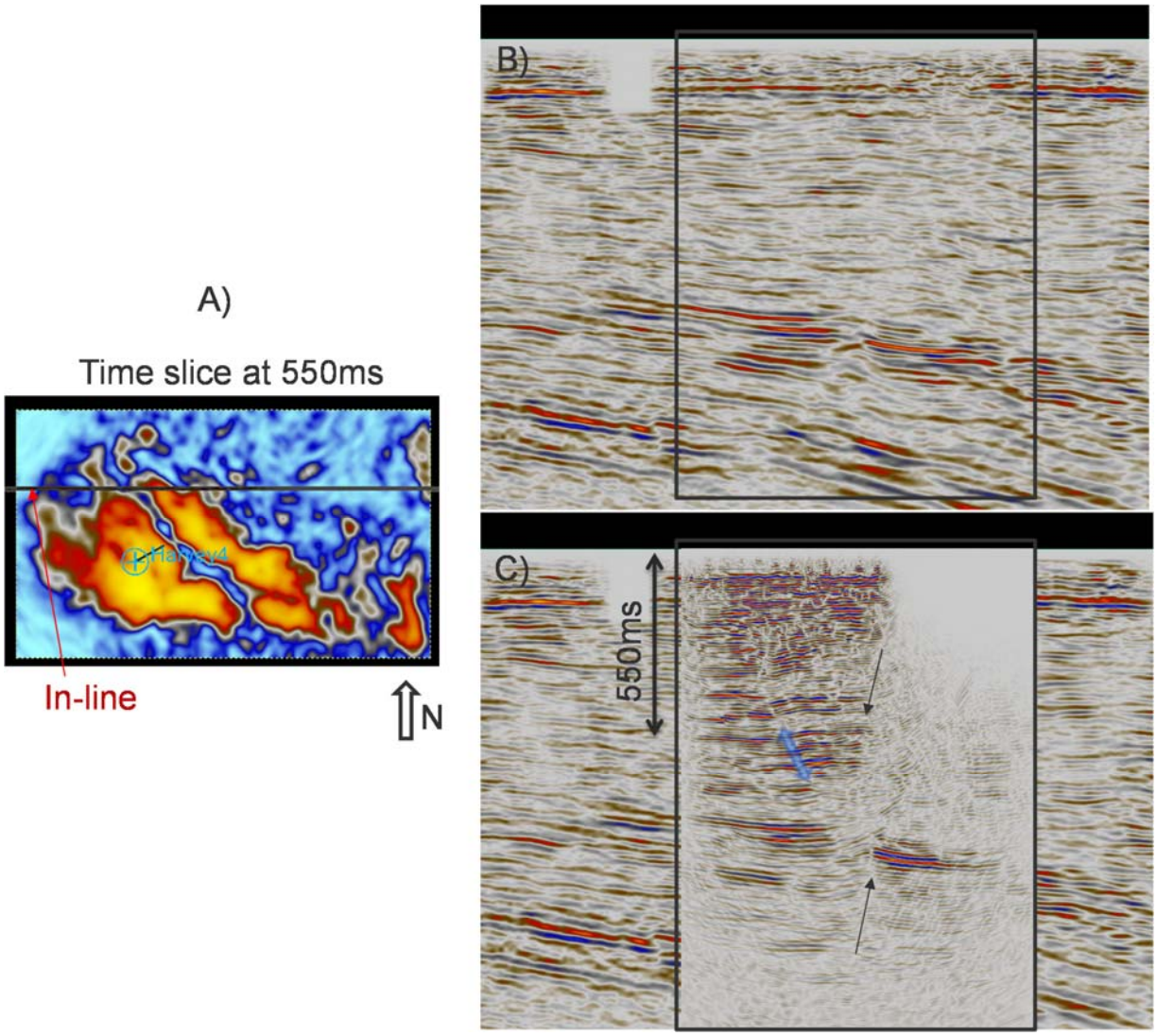

Figure 18. 3D survey comparison: A) Time slice through similarity section, B) Regional Harvey 3D and C) Nested 3D (PSTM cube) inserted into the rectangular area. The location of the inline section shown is marked in A). The blue transparent double arrow is used to denote “new” faults, not seen in the regional data. The black arrow denotes where fault is expressed with much better clarity in the Nested 3D.

Preliminary fault distribution analysis

A number of fault expressions were analysed in time slice domain but also cross-section using PSTM AGC and PRA cubes. Both processing products; the amplitude non-preserved PSTM seismic cube (AGC scaled) and the amplitude-preserved seismic cube (PRA) were used for the analysis of fault expression in terms of continuity of fault trace and its reflectivity. Additional information and improved fault trace identification was achieved with a similarity cube. Such an example is shown in Figure 19 where horizontal intersections through amplitude and similarity cubes are compared. Faults of different scales or orders can be seen in these two displays. Both displays should be used concurrently as some faults are better expressed in one domain rather than the other.

When analysing the vertical planes i.e. in-line and cross-line sections, we observed the presence of numerous medium size and small through faults. They can be recognised in either AGC or PRA cubes although very shallow structures are better expressed in the PRA cube. Fault traces can be further enhanced through the application of instantaneous attributes. An example is shown in Figure 20 where in-line and cross-lines are taken from the Perigram cube. This attribute is a product of reflection continuity and low-pass filtered reflection strength or envelope. In these displays we can clearly trace faults of different orders (scales). In panel 4 of Figure 20, or in-line 110, (S-N direction) we can identify a small throw fault, with the displacement of about 10m or less at 550 m depth. A trace of this fault can be mapped over a considerable depth extent.

In Figure 21, on cross-lines, in W-E direction, we can identify numerous small throw faults. In panel 2 of Figure 21, or cross-line 50, we can identify at least 4 faults with the through of 20 m or larger. Fault traces are very well imaged down to 1.1 s, which approximately corresponds to 1.5 km depth. The display scale is exaggerated to enhance discontinuities.

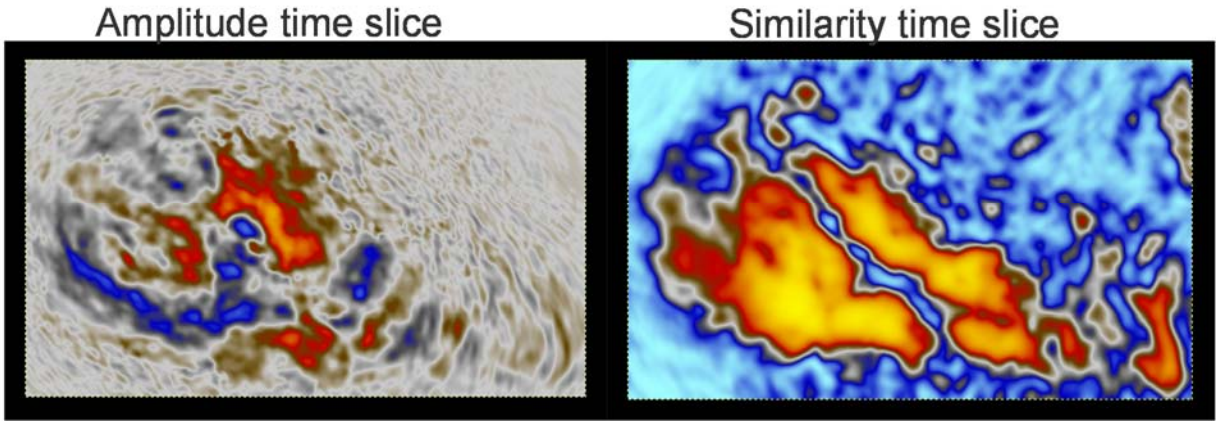

Figure 19. Time slice from the: amplitude cube (left) and similarity cube (right). The main faults can be seen tracking from top left to bottom right as a blue linear trend with the orange area of the similarity time slice. It is in a similar location but of lower fidelity in the amplitude time slice.

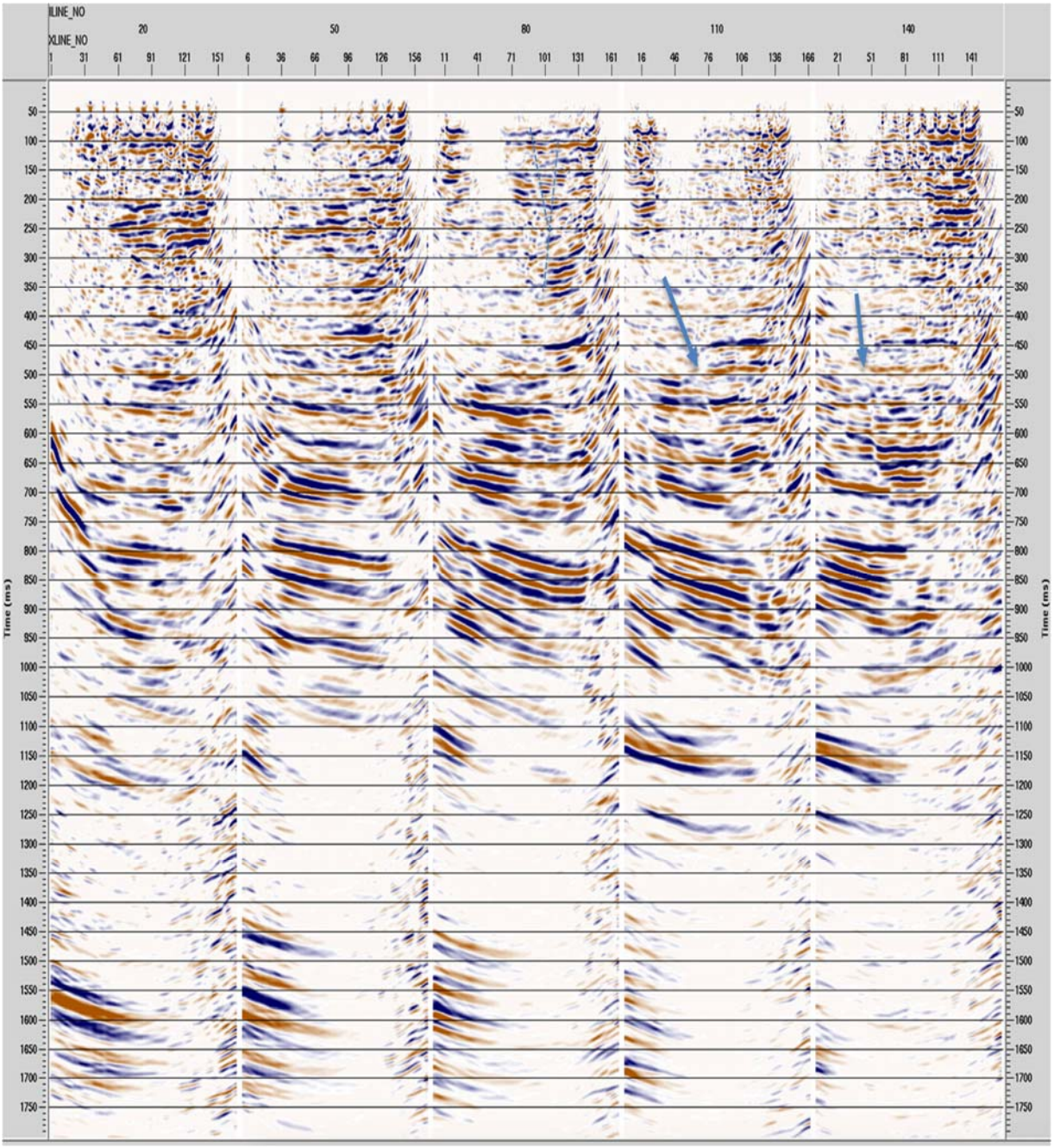

Figure 20. Perigram cube: a number of parallel in-lines are shown. The blue arrows indicate some of the larger fault traces. The blue dashed lines denotes very shallow, smaller faults.

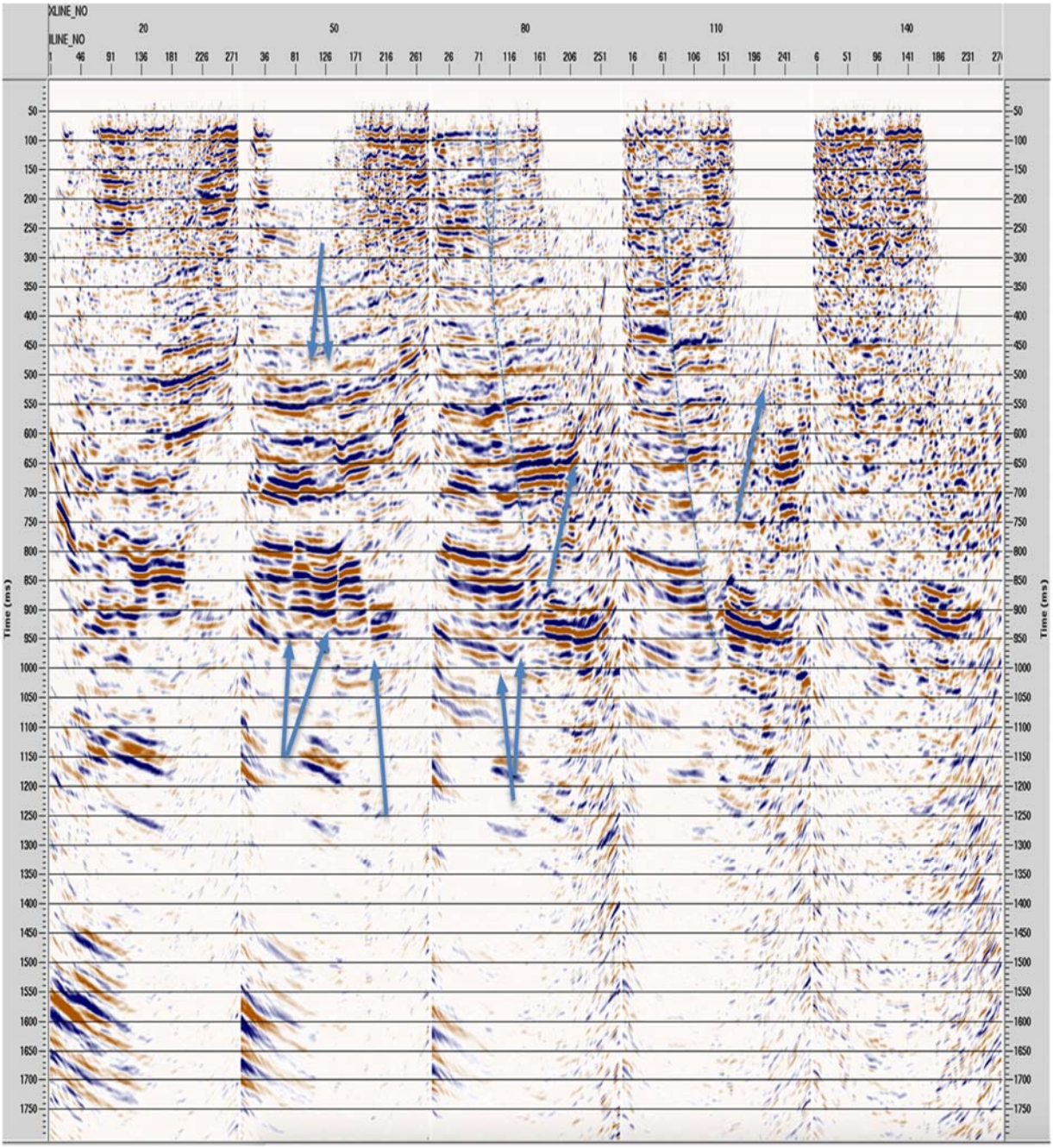

Figure 21. Perigram cube: cross-lines shown. The blue arrows indicate some of the larger fault traces. The blue dashed lines denotes very shallow, smaller faults. Fault complexity is fully expressed in this direction.

Conclusions and recommendations

The high resolution Harvey Nested 3D seismic data has been acquired with the National Geosequestration Laboratory (NGL) using a state-of-the-art hybrid recording system. Two light NGL vibrator trucks (UNIVIB) with extra-wide tires were deployed in a “flip-flop” shooting pattern. No foot print was left in the ground by this seismic source vehicle. A small seismic crew comprising of 8 people, managed the deployment of 2,300 channels with ease and fired close to 1600 shots in 4.5 days. The single long-duration sweeps and a single sensors, combined with the achievements of a high fold produced very good quality data of high quality signal to noise ratio. Preserved amplitude processing and pre-stack imaging proved to be a very effective processing approach for structural analysis. The same data can be used in the near future for more qualitative studies involving acoustic inversion and AVO studies after calibration to the Harvey-4 well logs.

The Nested 3D data cube was inserted into the large, regional scale Harvey 3D survey. A comparative analysis showed the following:

- Several faults are seen in the Nested 3D data, which were not previously identifiable in the regional 3D cube. This includes faults at different scales.
- All discontinuities (large and small) are of a much higher fidelity in the Nested 3D survey
- Some faults appear to propagate near to the surface but are of a small scale throw
- Faulting in the area has a high complexity
- The Harvey 4 well appears to have drilled through a fault of a large throw (several tens of metres). Further structural interpretation of the high-resolution cube is highly desirable.

These results demonstrate clearly that high-resolution surveys are important for imaging the top 1,000 m of sediments. The Nested 3D survey produced higher fidelity imaging of faults down to at least 1,500 m in comparison to the regional 3D data.

It can be further concluded that in certain geological scenarios, a higher resolution seismic data are necessary for adequate fault characterisation and reservoir studies needed for future CO_2 sequestration projects.

The fault density and complexity cannot be fully realised with the low-resolution seismic data even at greater depths. Low-resolution data are also not appropriate for the implementation of seismic stratigraphy and quantitative interpretations. It is thus recommended that high resolution surveys, similar to the Nested 3D survey, are conducted at the site of future boreholes prior to drilling in order to: a) optimise their position through better fault location prediction and b) enable accurate structural and stratigraphic studies of direct importance to dynamic simulations and reservoir studies, including CO_2 sequestration monitoring. The cost of the Nested survey conducted is only a fraction (less than 15%) of the drilling cost but the impact can be significant in terms of borehole relocation, fault correlation and dynamic simulations. Fault geometry and their lateral extent away from the well can only be inferred from such high-resolution 3D seismic data. It is

to expect that drilling and logging also identified the same small faults identified in seismic cubes around the Harvey 4 well.

The long broadband sweeps inject high frequencies at shallow depths. Hence they are superior in providing high-resolution images in comparison to stacking shorter sweeps. The new broadband seismic vibrating source proved to be also quite powerful. It generates enough energy to clearly record events from depths of at least 1500 m, as verified in the current data. A larger size high-resolution seismic survey would most likely show that the penetration depth with the currently used recording parameters is closer to 2,500 m. This cannot be explicitly verified from the present cube due to a low data fold away from the central point.

All of the field equipment utilised for this survey was acquired under the EIF grant scheme to the National Geosequestration Laboratory (NGL) consortium (CSIRO, Curtin, UWA). The equipment and the approach used in this project provide a low footprint, low impact option for acquiring seismic data in areas that have public concern regarding the surface environmental disturbance, yet still have the capacity to obtain high resolution images to reservoir depth. Such surveys may get a wider public acceptance in Harvey area.

Future work with the acquired data is likely to involve well ties using Harvey-4 logs, followed by acoustic inversion and refined analysis and interpretation.

Further studies of the shallow structures will continue through utilisation of VSP data and the horizontal component data.

References

Audebert, F. L., and P. Froidevaux, 2005, Regularization of illumination in angle domains - a key to true amplitude migration: The Leading Edge, **24**, 643-654.

Deregowski. S.M. 19H2. Dip-Moveout and Reflector Point Dispersal. Geophysical Prospecting **30**.31 H-322.

Ferber, R. G., Sanders, B., and Yilmaz, O., 1996, Quick-look 3-D prestack time migration: 66th Ann. Internat. Mtg., Soc. Expl. Geophys., Extended Abstracts, 451-545.

French, W., 1975, Computer migration of oblique seismic reflection profiles: Geophysics, 40, 961-980.

Gardner, G. H. F., French, W. S., and Matzuk, T., 1974, Elements of migration and velocity analysis: Geophysics. 39, 81 1-825.

Hatherly, P., Urosevic, M., Lambourne, A., and Evans, B. J., 1994, A simple approach to calculating refraction statics calculations: Geophysics: 59, 156-160.

Kangan F., 1995, Prestack Kirchhoff migration: CREWES Research Report – Volume 7, 31.

Langhi, L. , Zhang, Y. , Nicholson, C., , Bernardel, G., Rollet, N., Schaubs, P., Kempton, R., and Kennard, J., 2012, Geomechanical modelling of trap integrity in the northern offshore Perth basin; CSIRO Open file report: EP 12425.

Mayne, W. H., 1962, Common reflection point horizontal data stacking techniques: Geophysics, 27, 927-938.

Schneider, W. A., 1978, Integral formulation for migration in two and three dimensions: Geophysics, 43, 49-76.

Taner , M. T., and Koehler, F., 1981, Surface consistent corrections: Geophysics, 46, 17-22.

M. Urosevic, S. Ziramov, R. Pevzner and A. Kepic, 2014, Harvey 2D test seismic survey-issues and optimisation: ANLEC R&D Project 7-1213-0223.

Yilmaz, O. 1987. Seismic data processing/Ozdogan Yilmaz. Tulsa, OK: Society of Exploration Geophysicists.

http://www.sercel.com/products/Lists/ProductSpecification/Unite_brochure_Sercel.pdf

http://www.sercel.com/about/Pages/history.aspx